NASA TECHNICAL NOTE NASA TN D-3185

NASA TN D-3185

CONDENSATION PRESSURE DROP OF NONWETTING MERCURY IN A UNIFORMLY TAPERED TUBE IN 1-g AND ZERO-GRAVITY ENVIRONMENTS

by James A. Albers and Robert P. Macosko

Lewis Research Center
Cleveland, Ohio

NATIONAL AERONAUTICS AND SPACE ADMINISTRATION • WASHINGTON, D. C. • JANUARY 1966

NASA TN D-3185

CONDENSATION PRESSURE DROP OF NONWETTING MERCURY IN A UNIFORMLY TAPERED TUBE IN 1-g AND ZERO-GRAVITY ENVIRONMENTS

By James A. Albers and Robert P. Macosko

Lewis Research Center
Cleveland, Ohio

NATIONAL AERONAUTICS AND SPACE ADMINISTRATION

For sale by the Clearinghouse for Federal Scientific and Technical Information
Springfield, Virginia 22151 – Price $2.00

CONDENSATION PRESSURE DROP OF NONWETTING MERCURY IN A UNIFORMLY TAPERED TUBE IN 1-g AND ZERO-GRAVITY ENVIRONMENTS

by James A. Albers and Robert P. Macosko

Lewis Research Center

SUMMARY

An experimental investigation was conducted to determine the pressure drop of nonwetting (dropwise) condensing flow of mercury vapor in 1-g and zero-gravity environments. Local static pressure data were obtained for a uniformly tapered stainless-steel horizontal tube for various flow rates, pressures, and condensing lengths.

The overall static pressure difference from inlet to interface $(P_0 - P_{liq})_s$ varied from a pressure rise of 0.9 pound per square inch to a pressure drop of 0.1 pound per square inch, while the overall total pressure drop varied from 0.0 to 1.4 pounds per square inch for the condensing lengths and flow rates investigated. The experimental data indicated that the gravity effect was negligible for all flow rates investigated.

Lockhart-Martinelli correlation predicted values for the ratio of pressure gradients Φ_g within approximately ±35 percent for the high quality region of the condensing tube. The experimental values of the ratio of pressure gradients Φ_g ranged up to five times the value predicted by Lockhart-Martinelli for the low quality region of the tube. The fog-flow theory of Koestel, et al., roughly predicted the trend of the data over the entire quality range. Experimental values of the fog-flow parameter $\Phi_g^2 x^{3/4}$ varied between -50 and +100 percent of the theoretical value for Weber numbers ranging from 10 to 100 (high velocity region). For Weber numbers ranging from 0.1 to 10 (low velocity region) the experimental values varied between -50 and +165 percent of the theoretical value.

INTRODUCTION

The flow characteristics of working fluids in the absence of body forces are among the numerous problems encountered in the design of components of Rankine cycle turbo-

generator systems. Knowledge of zero-gravity flow phenomena is of particular importance in the design of those components in which the working fluid experiences phase changes such as occur in the condensing process. These phase changes represent a major problem in the design of condenser components with regard to the prediction of pressure drop. Furthermore, the existing data on pressure drop in a 1-g environment may not be representative of the pressure drop during system operation in a weightless environment. The pressure drop in a condenser tube is influenced by the flow regimes encountered. Previous photographic studies at the Lewis Research Center indicated differences in the drop distribution of nonwetting mercury condensing in straight tubes in 1-g and zero-gravity environments (ref. 1). Under 1-g conditions droplet runoff down the tube wall was observed, resulting in a liquid accumulation in the bottom of the tube, particularly in the low velocity region. Under zero-gravity conditions, the liquid droplets were uniformly distributed around the circumference of the tube and in the vapor stream. These flow differences may influence the pressure drop in the condenser tube, which, in turn, is important to the design of mercury condensers. As part of the overall mercury condensing program at NASA Lewis Research Center, the effect of weightlessness on the pressure drop of nonwetting mercury condensing in constant diameter and uniformly tapered tubes was studied. The zero-gravity durations were obtained in a converted Navy bomber (AJ-2) (fig. 1) flying through a Keplerian trajectory. The effect of weightlessness on the pressure drop of mercury condensing in a constant diameter tube was reported in reference 1. A continuation of this study is reported herein. Because tapered tubes are currently being considered for use in condensers, particular emphasis was given to the local pressure distribution and overall pressure difference (from inlet to interface) in a tapered tube. This investigation compares the local pressure gradients

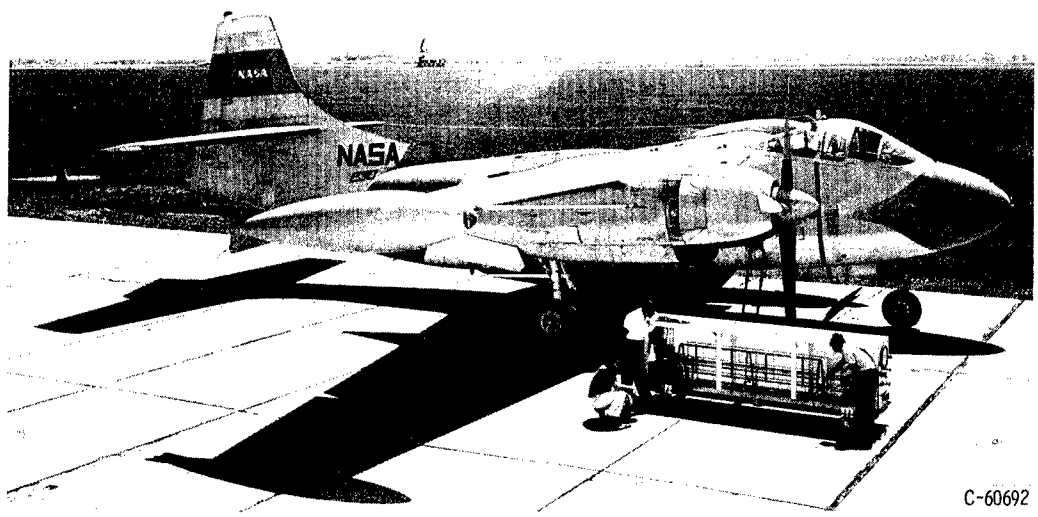

Figure 1. - Zero-gravity flight facility.

with the analytical predictions of Lockhart-Martinelli and of Koestel et al. as discussed in references 2 and 3, respectively.

Previous analytical studies of the two-phase flow problem have dealt with the simplified flow models to derive correlations that would permit the estimation of two-phase pressure drops (from single-phase pressure drop measurements). Lockhart-Martinelli pressure drop correlations for two-component, two-phase, adiabatic flow are often applied to condensing (ref. 2). Lockhart-Martinelli relates the ratio of the two-phase frictional pressure gradient to the pressure gradient of the vapor flowing alone. Both Hays (ref. 4) and Kiraly (ref. 5) compared mercury condensing data with the Lockhart-Martinelli correlations. Hays found general agreement in the high quality region of the condensing tube. At low qualities the agreement with theory was not apparent. Kiraly's values also showed considerable deviation from Lockhart-Martinelli for condensation inside horizontal tapered tubes and inclined tubes of constant diameter.

Another correlation used for condensing is the fog-flow correlation reported in reference 3. This correlation assumes homogeneous flow and accounts for the reduction in flow area due to the condensed droplets on the tube inside surface. The local Weber number (which is a function of this reduction) is used to determine the ratio of the two-phase frictional pressure gradient to the pressure gradient that would result if the vapor flowed alone. Comparison of the existing data obtained by the authors of reference 3 with the fog-flow correlation showed that the theory satisfactorily predicted the trend of the data although considerable scatter was present.

An analysis of the phenomena involved in condensing under differing gravity conditions can be found in reference 6. Mercury-nitrogen two-phase flow data were presented with the test section positioned in different orientations. The authors concluded that pressure drop can be expected to change when going from 1 g to zero gravity under limitations of Reynolds number and vapor specific volume.

SYMBOLS

A cross-sectional area, sq ft

$\overline{A}$ average cross-sectional area, sq ft

c_p specific heat of mercury vapor, Btu/(lb mass)(^{o}F)

D tube outside diameter, ft

d tube inside diameter, ft

f friction factor, dimensionless

f function of

g_c conversion factor, 32.174 (lb mass)(ft)/(lb force)(sq sec)

h local heat transfer coefficient, Btu/(sec)(sq ft)(^{o}F)

h_{fg} mercury latent heat of vaporization, Btu/lb mass

k thermal conductivity, Btu/(sec)(ft)(^{o}F)

L length, ft

ℓ distance from condensing tube inlet, ft

Nu Nusselt number, dimensionless

P pressure, lb/sq ft

PT pressure transducer

q local heat flux, Btu/(sec)(sq ft)

$\overline{q}$ average heat flux, Btu/(sec)(sq ft)

Re Reynolds number, dimensionless

T temperature, ^{o}F

t time, sec

u velocity, ft/sec

V velocity ratio, u_{liq}/u_g, dimensionless

v specific volume, cu ft/lb mass

We Weber number, dimensionless

w mass flow rate, lb mass/sec

x quality, w_g/w_T, dimensionless

μ viscosity, lb mass/(ft)(sec)

ρ density, lb mass/cu ft

$\overline{\rho}$ average density, lb mass/cu ft

σ surface tension, lb force/ft

Φ_g Lockhart-Martinelli parameter, $\sqrt{(\Delta P/\Delta L)_{TPF}/(\Delta P/\Delta L)_g}$, dimensionless

χ two-phase flow modulus, $\sqrt{(\Delta P/\Delta L)_{liq}/(\Delta P/\Delta L)_g}$, dimensionless

Subscripts:

c condensing

e exit

g	mercury vapor
l	local
liq	liquid
N_2	Nitrogen coolant
S	static
sat	saturated mercury vapor
sup	superheated mercury vapor
T	total
TP	two-phase
TPF	two-phase frictional
t	tube
tt	turbulent liquid, turbulent gas
vt	viscous liquid, turbulent gas
w	wall
0	inlet
0, 12, 36 48, 60, 72	distance from condensing tube inlet, in.

DESCRIPTION OF APPARATUS

Experimental System and Components

Schematics of the experimental system and components are presented in figures 2(a) and (b). Photographs of the system components are shown in figures 2(c) and (d). For simplicity, a single pass mercury system, with a capacity for a 90-minute continuous run, was designed. The weight of the test package and related power equipment was approximately 2000 pounds. The mercury system consisted of an expulsion cylinder, a liquid-flow measuring system, a preheater, a high-heat-flux boiler, and a main boiler, a vapor flow measuring venturi, a horizontal condensing tube, and a receiver for collecting the condensed mercury. The condensing tube was cooled by gaseous nitrogen jets flowing through 0.052-inch holes every 3/4 inch along two diametrically opposed manifolds located above and below the condensing tube. The nitrogen jet orifices in the cooling manifolds were approximately 1 inch from the centerline of the condensing tube.

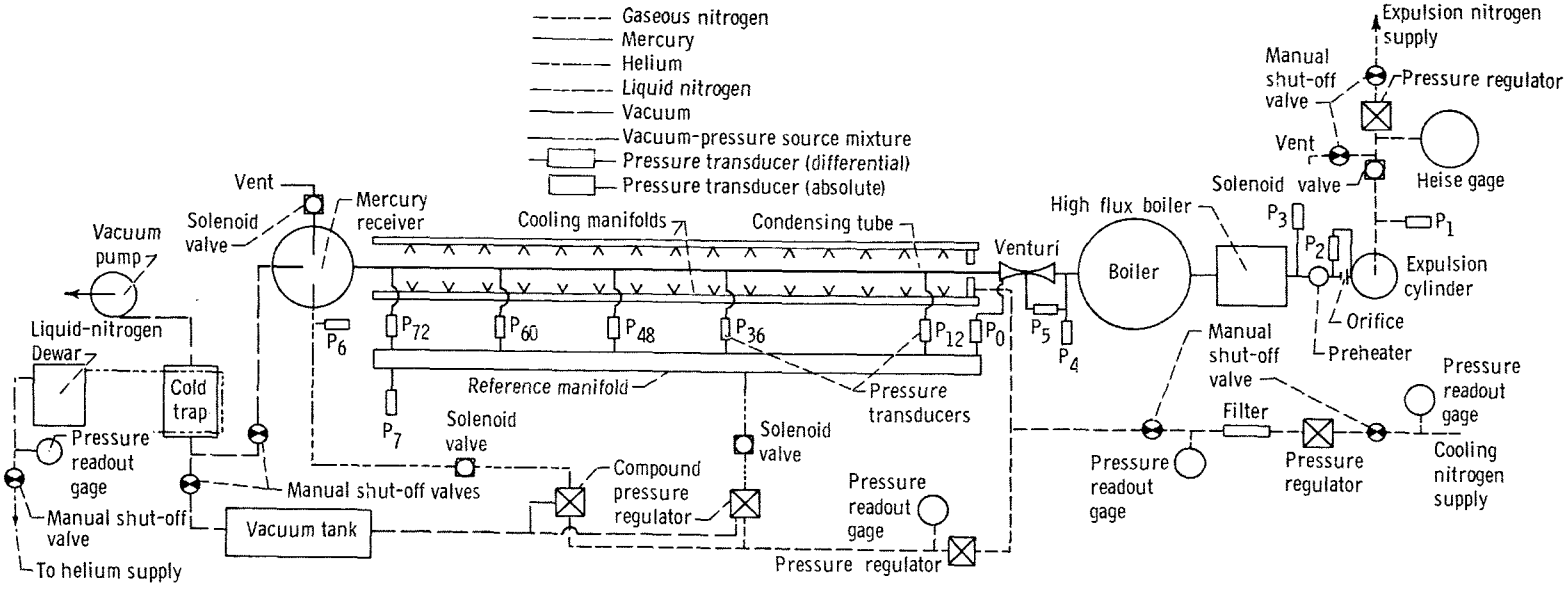

(a) Schematic drawing of system.

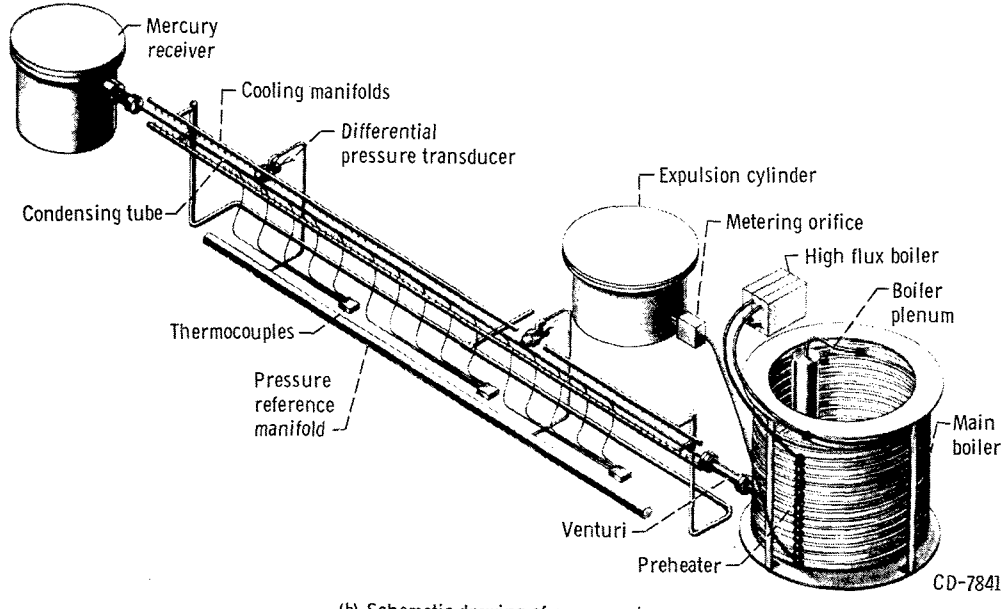

(b) Schematic drawing of components.

Figure 1. - Experimental system and components for crossflow-nitrogen-cooled condenser.

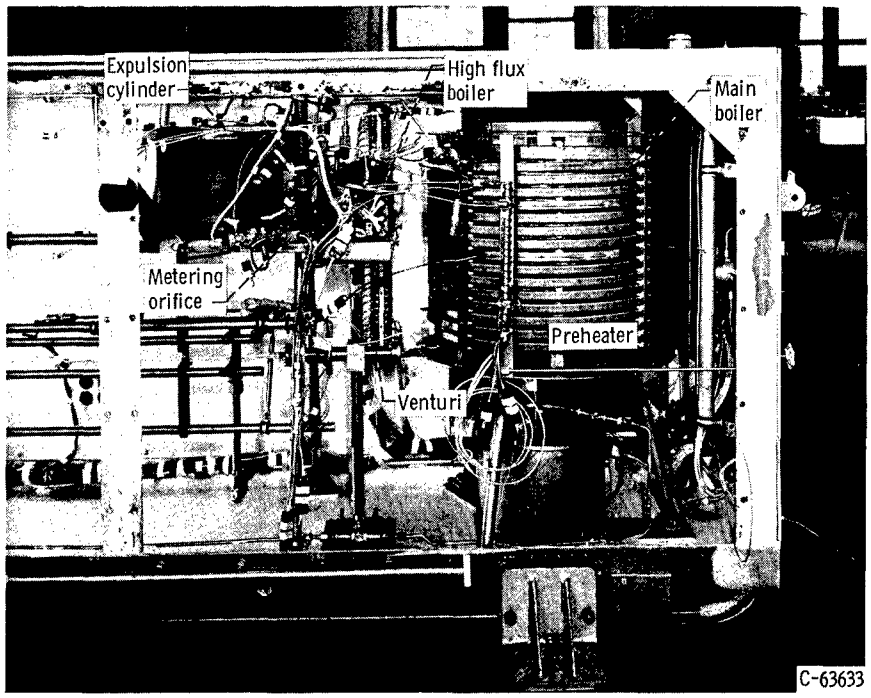

(c) Boiler end of experimental package.

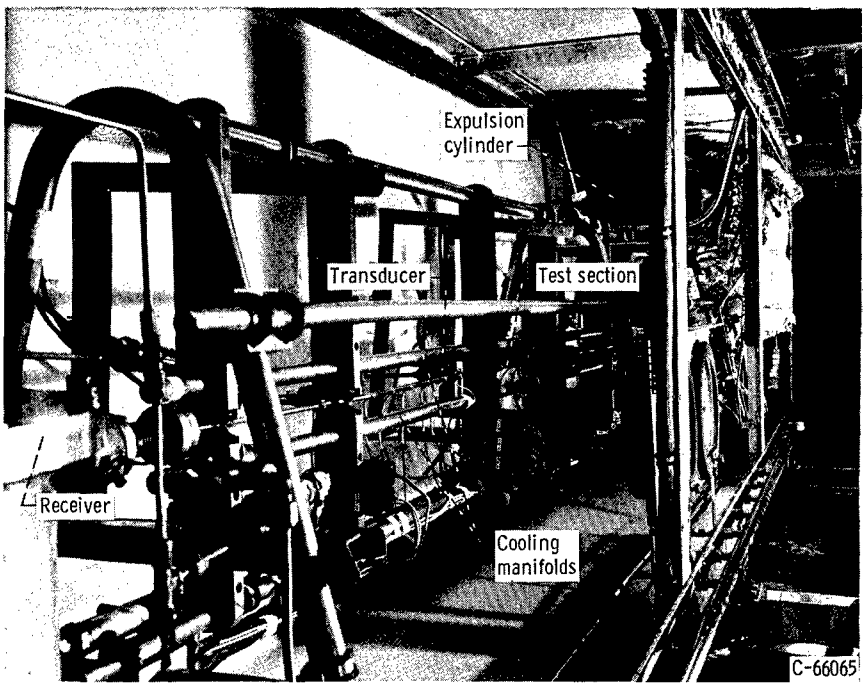

(d) Receiver end of experimental package.

Figure 2. - Concluded.

Approximately 250 pounds of triple-distilled mercury were stored in a stainless-steel expulsion cylinder. A neoprene bladder was used in the cylinder to maintain the orientation of the mercury in the container during the zero-gravity maneuver.

Boiling was accomplished in three stages. Mercury was first passed through a preheater, which raised the liquid temperature to the saturation point. It then entered the high heat flux unit where nucleate boiling raised the vapor quality to approximately 25 percent. The additional heat input needed to increase the quality to about 90 percent was supplied in the main boiler, which consisted of a single 150-foot length of flattened tubing coiled in a 2-foot diameter helix. The power for the main boiler was applied directly to the tubing that formed the mercury flow passage. The helical design of this unit, which created very high lateral gravity forces on the vapor, minimized the effect of the varying vertical gravity forces encountered during the transition from 1 g to zero gravity.

The mercury vapor flow into the condenser was measured by a venturi at the condenser inlet, which had a throat diameter of 0.277 inch and an exit diameter of 0.311 inch. The condenser was an 84-inch-long uniformly tapered stainless-steel (AISI 316) horizontal tube with a 0.40-inch inside diameter at inlet and a 0.15-inch inside diameter at outlet with a 0.025-inch wall thickness. A pressure tap was located at 0, 12, 36, 48, 60, and 72 inches from the tube inlet. The exit of the condenser was equipped with a 1/16-inch-diameter orifice to help damp out potential instabilities in the tube.

The mercury receiver consisted of a cylinder baffled on the inside to minimize mercury movement during the zero-gravity maneuver. Receiver operating pressure was maintained at about 15 pounds per square inch absolute by a nitrogen gas pressure regulator.

Instrumentation

The location of instrumentation of the condenser tube is shown in figure 3. Stainless-steel inductance-type (linear variable differential transformer) pressure transducers, capable of operating in a mercury environment up to 900° F, were used to measure condenser tube pressure distribution, venturi inlet pressure, and venturi pressure drop. Each transducer in direct contact with mercury was mounted with its core axis parallel to the lateral axis of the aircraft to minimize the effects of the zero-gravity maneuver. Differential pressure transducers used on the condensing tube were mounted with the higher pressure sides to the tube and the low pressure sides referenced to a common, nitrogen gas manifold. These pressure transducers were connected directly to fittings which were welded to the condenser tube. Low temperature variable reluctance transducers were used at all other locations in the system. A complete listing of all pressure transducers and their respective calibration range is presented in table I.

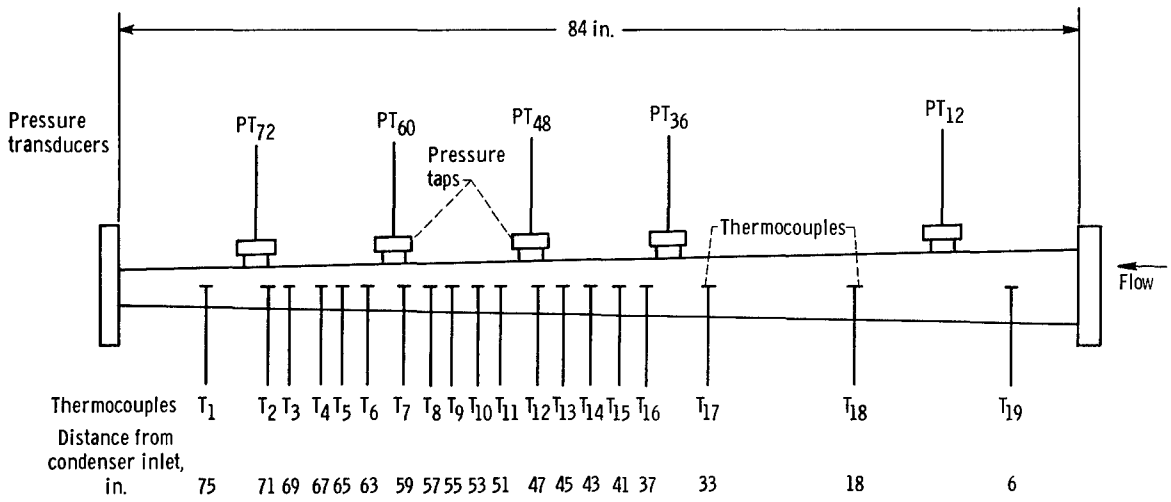

Figure 3. - Location of instrumentation on condensing tube (uniformly tapered stainless-steel tube with 0.40 in. i.d. at inlet, 0.15 in. i.d. at outlet, and 0.025 in. wall thickness).

Thermocouples throughout the system were constructed of the Instrument Society of America (ISA) standard calibration K (Chromel-Alumel) wires. A shielded, sheathed thermocouple was immersed in the mercury vapor stream at the venturi inlet. Thermocouples were spotwelded to the outside wall of the condenser and were used for indicating the location of the interface.

All temperature and pressure data needed for the analysis were recorded on two multichannel oscillographs. A typical oscillograph trace showing the vertical accelerations during the maneuver and pressure oscillations in the condenser is presented in figure 4 (p. 10). The accelerations generated along the three axes of the aircraft were sensed by accelerometers located in the bomb bay near the geometric center of the experiment. The gravity levels experienced here were relayed to readout equipment on the pilot's control panel and were used for aircraft control throughout the maneuver. The same gravity levels were recorded on the pressure oscillograph so that a direct comparison with system pressures could be made.

PROCEDURE

The zero-gravity durations were obtained in a converted Navy bomber (AJ-2) flying through a Keplerian trajectory. About 4 to 5 seconds of the trajectory were required to damp out pressure oscillations induced by the pullup maneuver. All the maneuvers flown during the test program were analyzed, and average zero-gravity times were computed. From these data it was shown that for an average of 5.28 seconds per trajectory, the gravity level was within ±0.01 g and for 12.72 seconds the gravity level was within ±0.05 g. The aircraft and zero-gravity maneuver is discussed in more detail in appen-

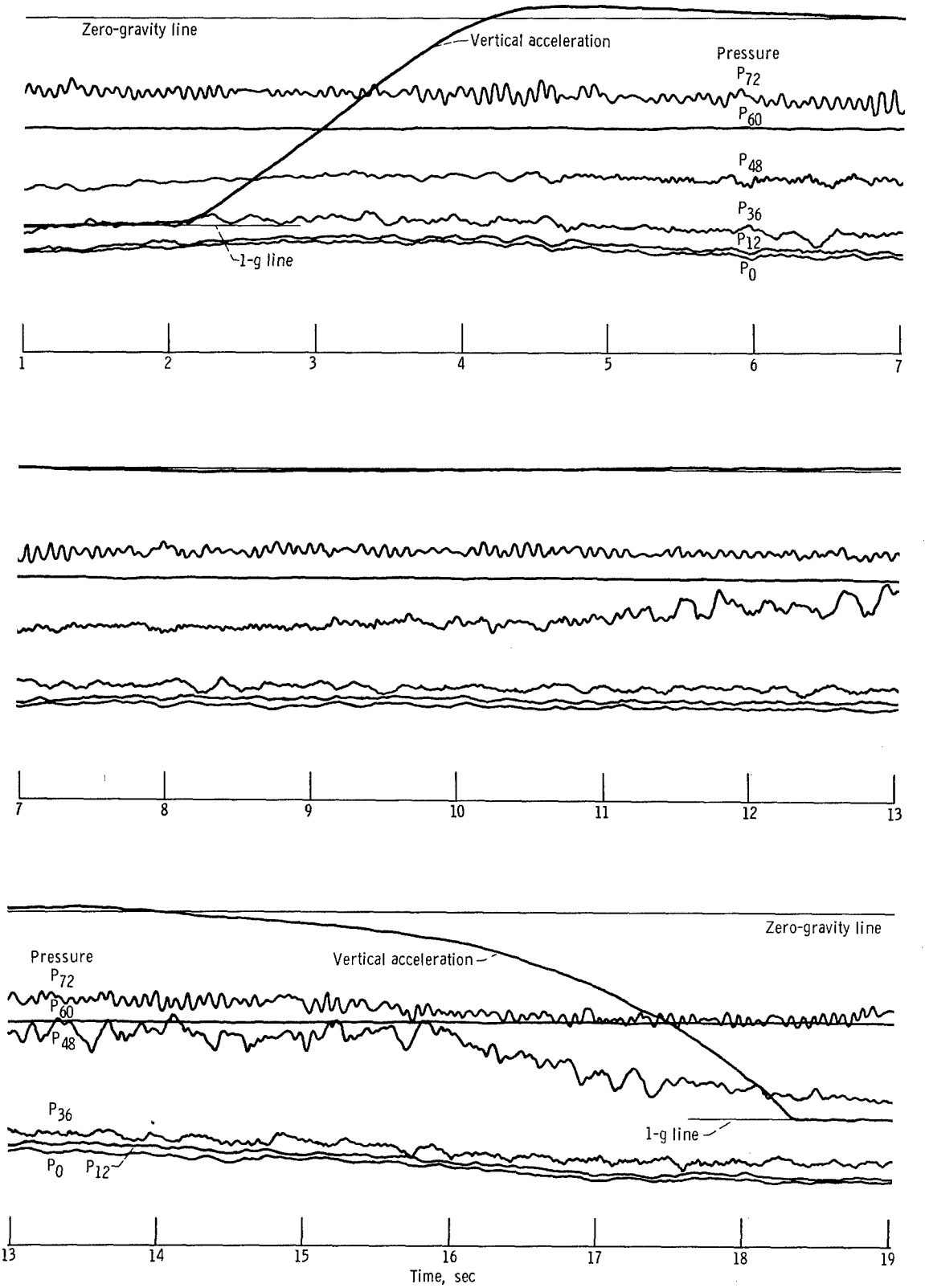

Figure 4. - Typical oscillograph trace.

dix A of reference 1.

A good comparison between 1-g and zero-gravity data points was obtained by taking the 1-g points in the aircraft while in level flight and the zero-gravity points immediately after without changing conditions. The aircraft accelerometers were zeroed with the condenser tube leveled to ensure good 1-g data while in flight. The zero-gravity data shown in table II was taken from oscillograph traces at points that represented the end of the longest segment of good zero-gravity.

Before initiating flow through the system, the mercury lines were evacuated to 0.06 torr and the mercury boilers brought to operating temperature. Mercury flow through the system was initiated and maintained by pressurizing the gas side of the bladder in the expulsion cylinder with regulated gaseous nitrogen. The liquid flow rate was monitored by observation of the pressure drop across a calibrated orifice located at the preheater inlet. Startup mass flow was set at 0.03 pound per second, and mercury vapor was allowed to purge the system for approximately 5 minutes to remove any remaining noncondensables from the lines. The receiver pressure was increased to a constant value (between 14 and 15 psia), and the nitrogen coolant flow was regulated to locate the interface at the desired location. During the 1-g and zero-gravity runs the tube skin temperatures were scanned using a manual selector switch to determine location of the interface within approximately ±1 inch. This was easily determined since the tube wall temperature dropped rapidly in the liquid region of the tube. Data were recorded for mercury mass flow rates of 0.025 to 0.05 pound per second, and condenser inlet vapor temperatures corresponding to approximately 300° F superheat. Boiler performance tests indicated low quality ($x \equiv w_g/w_T$) for vapor saturation temperature at the boiler outlet. It was necessary in this system to raise the vapor temperature to 300° F superheat to minimize liquid carryover.

Prior to every flight, a complete calibration of pressure and temperature instrumentation was carried out (see appendix A).

METHOD OF ANALYSIS

In the condensing process the static pressure drop is the sum of the frictional pressure drop and the pressure recovery (due to the momentum decrease). The frictional two-phase pressure drop between two pressure taps was determined by subtracting the calculated pressure recovery (due to momentum decrease) from the measured local static pressure difference. A force balance between two pressure taps of a tapered tube can be expressed as

$$(P_1 - P_2)_S \frac{\left(A_{t,1} + A_{t,2}\right)}{2} = -\frac{1}{g_c}\left(w_{g,1}u_{g,1} - w_{g,2}u_{g,2} + w_{liq,1}u_{liq,1} - w_{liq,2}u_{liq,2}\right) + F_{TPF} \tag{1}$$

where F_{TPF} is the mean force due to friction within the element and the subscripts 2 and 1 refer to points at one pressure tap and its preceding tap, respectively. If the liquid and vapor flow rates and the vapor velocity can be determined in equation (1), than an assumption of either the liquid velocity or the velocity ratio is required to obtain the change in momentum within the increment. The velocity ratio V is defined as the ratio of the liquid to the gas velocity

$$V = \frac{u_{liq}}{u_g}$$

For high velocity dropwise condensation (inlet vapor velocities on the order of 150 ft/sec) the drops that are entrained in the vapor stream are assumed to be accelerated very rapidly, approaching a velocity ratio of 1 ($u_{liq} = u_g$). This assumption is based on the analytical predictions of velocity profiles of liquid drops being entrained in the vapor stream (ref. 3).

If a velocity ratio of 1 is assumed, the two-phase frictional pressure gradient between two pressure taps is given by the expression (see appendix B)

$$\left(\frac{\Delta P_{TPF}}{\Delta L}\right)_{1,2} = \frac{(P_1 - P_2)_S \bar{A}_t - \frac{w_T^2}{\bar{\rho}_g g_c}\left(\frac{x_2}{A_{g,2}} - \frac{x_1}{A_{g,1}}\right)}{\int_{l_1}^{l_2} A_t dL} \tag{2}$$

The quality at any point along the condensing tube must be established to determine the two-phase frictional pressure gradient. For saturated conditions at the inlet, the quality is related to the local heat flux q by the following expression:

$$x = x_0 - \frac{\int_0^l q\pi D dL}{w_T h_{fg}} \tag{3}$$

But, for the test conditions considered, there existed approximately a 300° F superheat at the inlet of the condenser, which amounts to an additional heat load of 6 percent. A superheated vapor core with condensing on the tube surface was believed to exist. Observations based on unreported photographic studies at the Lewis Research Center of nonwetting condensation in glass tubes indicated that condensing begins very near the tube inlet. Jakob (ref. 7) and Kutateladze (ref. 8) indicated that it is not necessary that the entire mass of superheated vapor be cooled to the saturation temperature in order to initiate the condensation. The superheated vapor core is further believed to be distributed along the entire condensing length. From the preceding considerations and by the use of equation (3), the quality with superheated conditions at any point along the condensing tube is related to the local heat flux q by the following expression:

$$x = x_0 - \frac{\int_0^l q\pi D dL}{w_T\left[h_{fg} + c_p(T_{sup} - T_{sat})\right]} \tag{4}$$

By expressing the local heat flux in terms of the cooling-gas side heat-transfer coefficient, the quality at any point along the condensing tube is given by the following expression (see appendix C)

$$x = x_0\left(1 - \frac{1.61\left\{\left[D_0 - (D_0 - D_e)\frac{l}{l_e}\right]^{1.805} - D_0^{1.805}\right\}}{1.805\left\{\left[D_0 - (D_0 - D_e)\frac{l_c}{l_e}\right]^{0.805} - D_0^{0.805}\right\}(D_0 + D_c)}\right) \tag{5}$$

The method used to determine the inlet quality x_0 in equation (5) based on expressions derived by Murdock (ref. 9) are discussed in appendix D. By using equation (5), typical quality distributions as a function of length along the condensing tube can be calculated (fig. 5(a), p. 14). Taking into account the change in quality and diameter along the condensing tube results in a nonlinear decrease in vapor velocity (fig. 5(b)).

RESULTS AND DISCUSSION

The experimental data of this study are given in table II. The absolute local pressures along the test section are presented along with the mercury vapor stream temperature in the venturi inlet (approximate tube inlet temperature). The locations of the abso-

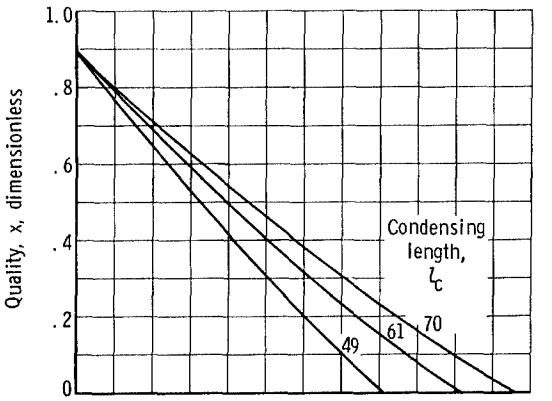

(a) Typical quality distributions for various condensing lengths.

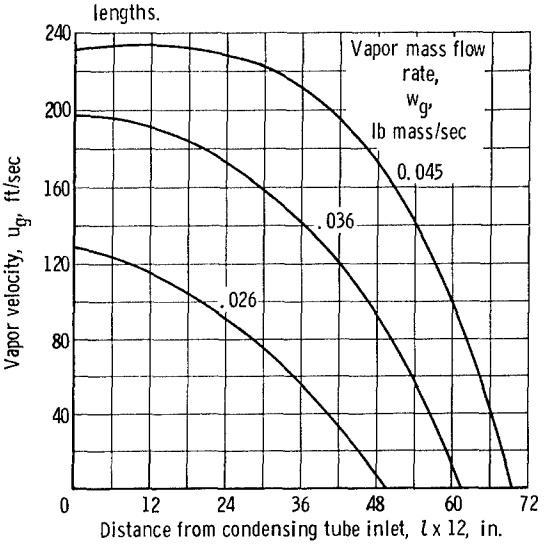

(b) Typical axial velocity distributions for various condensing lengths and flow rates.

Figure 5. - Typical quality and velocity distributions along condensing tube (inlet quality, x_0, 0.90).

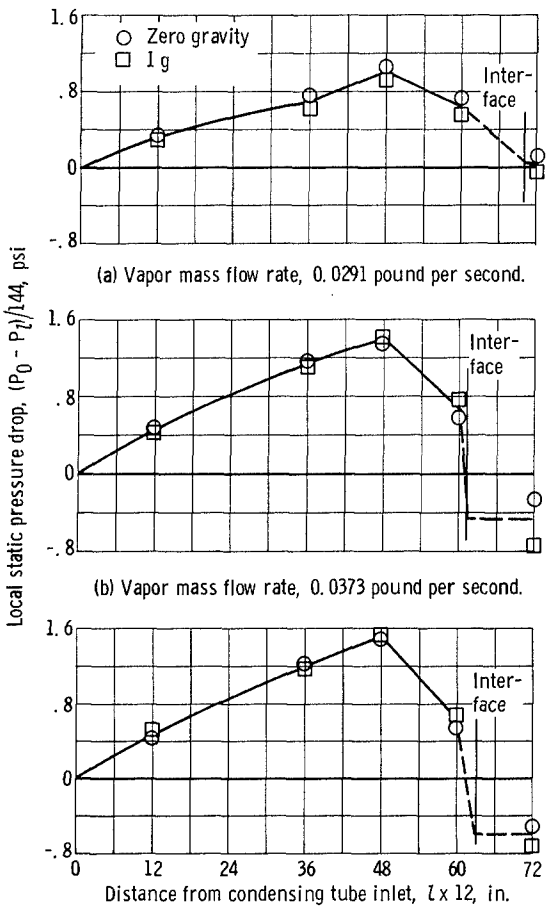

(a) Vapor mass flow rate, 0.0291 pound per second.

(b) Vapor mass flow rate, 0.0373 pound per second.

(c) Vapor mass flow rate, 0.0488 pound per second.

Figure 6. - Typical distributions of local static pressure drop for 1-g and zero-gravity environments.

lute pressures are identified by the subscripts to the letter P, which denote the distance from the inlet of the tube. The condenser inlet pressure P_0 was calculated from the venturi exit pressure and the losses due to the change in diameter from 0.31 inch (venturi exit) to the tube inlet diameter of 0.40 inch. The position of the liquid-vapor interface is given as the distance from the condenser inlet (condensing length). The calculated flow rates of the mercury liquid entering the boiler, the vapor flow rate out of the boiler, and the tube inlet quality are tabulated.

Measured Local Static Pressure Drop and Overall Pressure Difference

Typical distributions of local static pressure drop are presented in figure 6. These distributions were obtained from the difference between the inlet absolute pressure and

the measured absolute local static pressures along the condensing tube. A single curve was drawn because of the small spread between the 1-g and zero-gravity data points. This separation was within the accuracy of the instrumentation. In general, the local static pressure drop increased over the first half of the condensing length because of the high friction losses resulting from high vapor velocities and increased effective wall roughness caused by drop formation. In the last half of the condensing length, however, the pressure rise due to momentum decrease exceeds the pressure loss due to friction. This results in a net decrease in the local static pressure drop and, consequently, a relatively small overall static pressure rise. For the curves presented in figure 6 the inlet dynamic heads varied no more than 3 percent from each other. With the inlet conditions approximately the same there was no discernible difference between the distributions of local static pressure drop for 1-g and zero-gravity environments.

The effect of gravity on the measured overall static pressure difference $(P_0 - P_{liq})_S$ for various inlet velocities is presented in figure 7. The overall static pressure difference $(P_0 - P_{liq})_S$ was obtained by subtracting the average static pressure in the liquid leg from the inlet static pressure. Examination of figure 7 indicates little difference between the 1-g and zero-gravity conditions, although the majority of zero-gravity points fall slightly above the 1-g points. For condensing lengths from 45 to 71 inches and vapor inlet flow rates from 0.026 to 0.048 pound mass per second the values of $(P_0 - P_{liq})_S$ ranged between a pressure rise of 0.9 pound per square inch and a pressure drop of 0.1 pound per square inch.

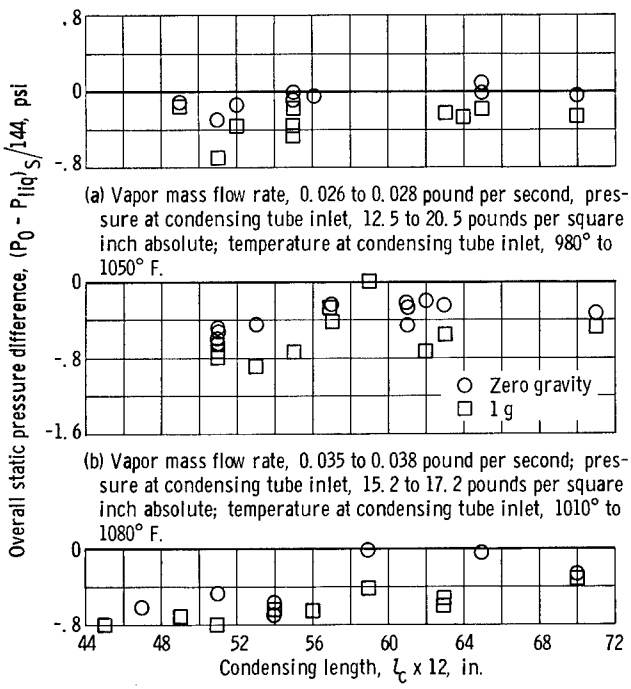

(a) Vapor mass flow rate, 0.026 to 0.028 pound per second, pressure at condensing tube inlet, 12.5 to 20.5 pounds per square inch absolute; temperature at condensing tube inlet, 980° to 1050° F.

(b) Vapor mass flow rate, 0.035 to 0.038 pound per second; pressure at condensing tube inlet, 15.2 to 17.2 pounds per square inch absolute; temperature at condensing tube inlet, 1010° to 1080° F.

(c) Vapor mass flow rate 0.044 to 0.048 pound per second; pressure at condensing tube inlet, 14.5 to 18.5 pounds per square inch absolute, temperature at condensing tube inlet, 1000° to 1100° F.

Figure 7. - Effect of gravity on overall static pressure difference.

The overall total pressure drop was obtained by adding the inlet dynamic pressure to $(P_0 - P_{liq})_S$, the dynamic pressure in the liquid portion being negligible (fig. 8, p. 16). The overall total pressure drop varied from 0.0 to 1.4 pounds per square inch for the condensing lengths and weight flows considered.

Comparison of Experimental Data with Lockhart-Martinelli Correlation

The Lockhart-Martinelli correlation relates two-phase frictional pressure gradient to the frictional pressure gra-

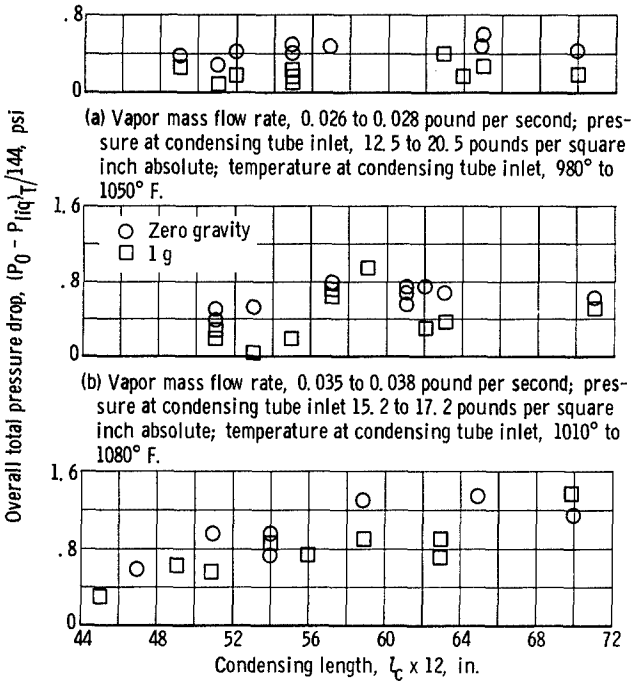

(a) Vapor mass flow rate, 0.026 to 0.028 pound per second; pressure at condensing tube inlet, 12.5 to 20.5 pounds per square inch absolute; temperature at condensing tube inlet, 980° to 1050° F.

(b) Vapor mass flow rate, 0.035 to 0.038 pound per second; pressure at condensing tube inlet 15.2 to 17.2 pounds per square inch absolute; temperature at condensing tube inlet, 1010° to 1080° F.

(c) Vapor mass flow rate 0.044 to 0.048 pound per second; pressure at condensing tube inlet 14.5 to 18.5 pounds per square inch absolute; temperature at condensing tube inlet, 1000° to 1100° F.

Figure 8. - Effect of gravity on overall total pressure drop.

dient of the gas alone. The correlation was based on data for isothermal two-phase, two-component flow in pipes. The Lockhart-Martinelli ratio of pressure gradients is a function of the parameter χ:

$$\chi^2 = \frac{\left(\frac{\Delta P}{\Delta L}\right)_{liq}}{\left(\frac{\Delta P}{\Delta L}\right)_g} \tag{6}$$

The preceding ratio can be calculated from the fluid properties and the vapor and liquid mass flow rates. This ratio depends on the flow mechanisms encountered. The frictional pressure drop data were compared to two flow mechanisms, that is, viscous liquid, turbulent gas, and turbulent liquid-turbulent gas where

$$\chi_{vt} = \left(\frac{16}{0.046} \frac{v_{liq}}{v_g} \frac{\mu_{liq}}{\mu_g} \frac{w_{liq}}{w_g}\right)^{0.5} Re_g^{-0.4} \tag{7}$$

$$\chi_{tt} = \left(\frac{w_{liq}}{w_g}\right)^{0.9} \left(\frac{v_{liq}}{v_g}\right)^{0.5} \left(\frac{\mu_{liq}}{\mu_g}\right)^{0.1} \tag{8}$$

To obtain the values of Lockhart-Martinelli parameters, v_{liq} and μ_{liq} were determined at the saturation temperature based on the average pressure in the tube. The determination of v_g was based on the pressure and temperature of the superheated vapor. Because μ_g is a function of temperature only, it was based on a saturation temperature equal to the temperature of the superheated vapor. The saturation properties were obtained from reference 10.

The experimental frictional pressure drop was compared to the Lockhart-Martinelli correlation for various flow rates, inlet pressures, and inlet temperatures to show the effect of gravity at a given flow rate (fig. 9). The gravity effect was negligible for all flow rates investigated.

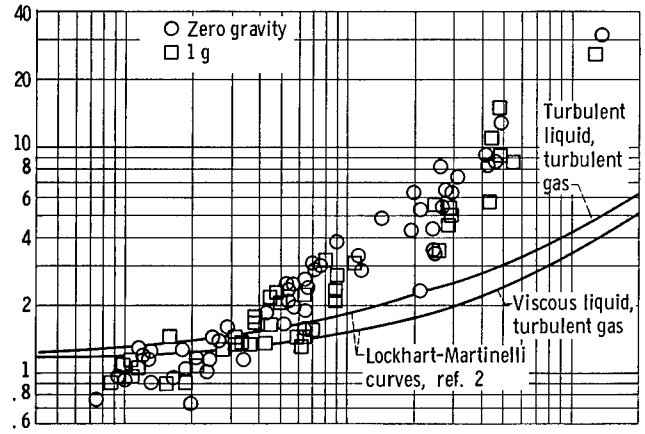

(a) Vapor mass flow rate, 0.026 to 0.028 pound per second; pressure at condensing tube inlet, 12.5 to 20.5 pounds per square inch absolute; temperature at condensing tube inlet, 980° to 1050° F.

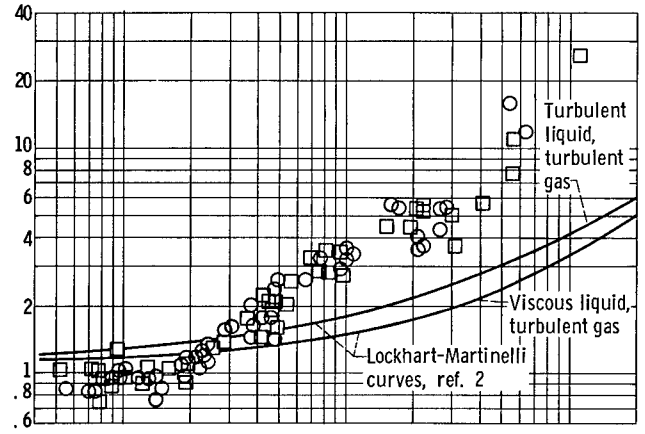

(b) Vapor mass flow rate, 0.035 to 0.038 pound per second, pressure at condensing tube inlet, 15.2 to 17.2 pounds per square inch absolute; temperature at condensing tube inlet, 1010° to 1080° F.

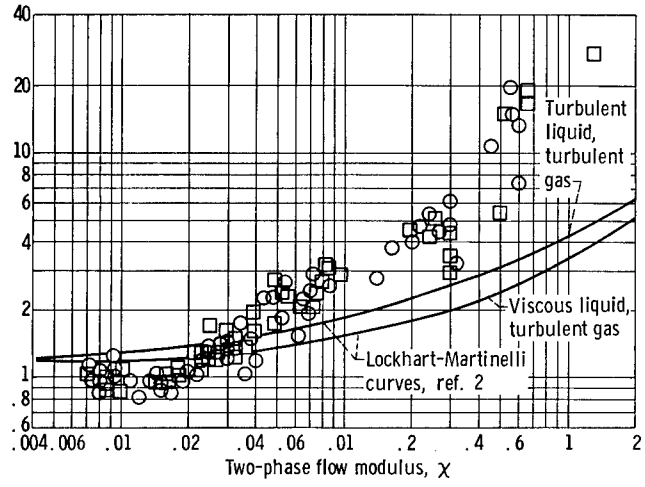

(c) Vapor mass flow rate, 0.044 to 0.048 pound per second; pressure at condensing tube inlet, 14.5 to 18.5 pounds per square inch absolute; temperature at condensing tube inlet, 1000° to 1100° F.

Figure 9. - Comparison of experimental data with Lockhart-Martinelli correlation.

The Lockhart-Martinelli correlation generally predicts Φ_g within approximately ±35 percent for the high quality, high vapor Reynolds number region of the condenser (i.e., low values of the parameter χ). The ratio of condensing pressure gradients Φ_g both for 1-g and zero-gravity ranged up to 5 times the value predicted by Lockhart-Martinelli for the low quality region of the tube (i.e., high value of the Lockhart-Martinelli parameter χ). A similar result is reported in reference 3. This deviation may result partly from the fact that the flow regimes in dropwise condensing are significantly different from the two-component, two-phase adiabatic flow model assumed by Lockhart-Martinelli. It can be concluded that the Lockhart-Martinelli correlation is not very applicable to condensing (with an approximately constant heat flux) over the entire quality range.

Comparison of Experimental Data with Fog-Flow Correlation

For high velocity condensing (inlet vapor velocity on the order of 150 ft/sec) the entrained drop size is considered to be on the order of 0.01 inch in diameter. The flow regime approaches a fog-flow condition in which the vapor and liquid can be treated as a homogeneous flow. The fog-flow regime of Koestel, et al., in

reference 3 is based on a zero-gravity flow model, and this correlation considers the reduction in the flow area due to the condensed droplets on the tube surface. This flow model assumes that a drop grows to a particular size called the critical drop diameter δ_c, which is then entrained in the vapor stream (ref. 3), where

$$d_m = d - 2\delta_c \tag{9}$$

and d_m is the diameter of the flow passage remaining when condensed drops form on the wall.

The fog-flow correlation expresses a fog flow parameter $\Phi_g^2 x^{3/4}$ as a function of Weber number

$$\Phi_g^2 x^{3/4} = f(We) = f\left(\frac{d\rho_g u_g^2}{2g_c \sigma_{liq}}\right) \tag{10}$$

Both the fog-flow parameter $\Phi_g^2 x^{3/4}$ and the Weber number are expressed as a function of the ratio of tube to fog-flow diameter:

$$\frac{d\rho_g u_g^2}{2g_c \sigma_{liq}} = \frac{8E_\sigma}{\left(\frac{d}{d_m}\right)^4 - \left(\frac{d}{d_m}\right)^3} \tag{11}$$

and

$$\Phi_g^2 x^{3/4} = \left(\frac{d}{d_m}\right)^{4.75} \tag{12}$$

where E_σ is an experimental constant (0.0464) that accounts for the effects of drop deformation, contact angle, and surface condition (ref. 6).

The theoretical relation between the fog-flow parameter and the Weber number was obtained from equations (11) and (12). Experimental values of We and $\Phi_g^2 x^{3/4}$ were calculated from the experimental pressure measurements and the local mercury conditions in the tube.

The experimental data were compared with the fog-flow theory for various flow rates, inlet pressures, and inlet temperatures (fig. 10). The gravity effect was negligible for all flow rates investigated.

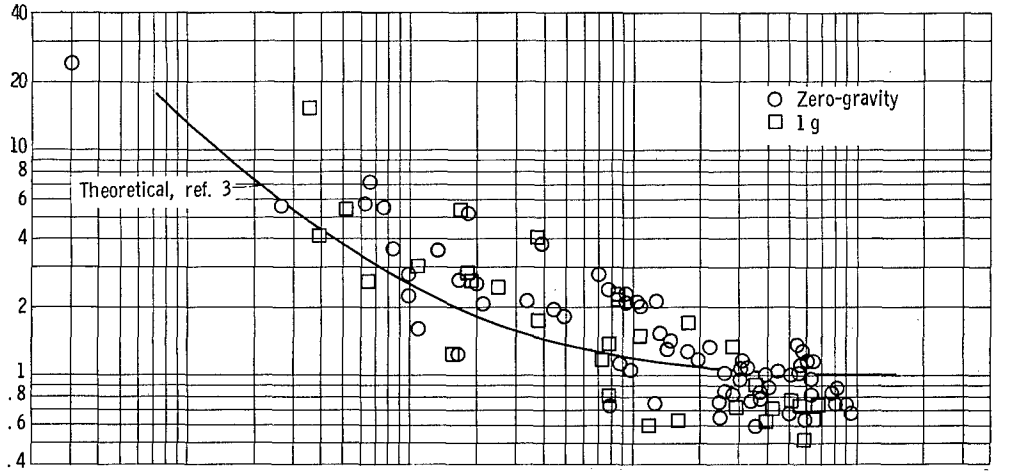

(a) Vapor mass flow rate, 0.026 to 0.028 pound per second; pressure at condensing tube inlet, 12.5 to 20.5 pounds per square inch absolute; temperature at condensing tube inlet, 980° to 1050° F.

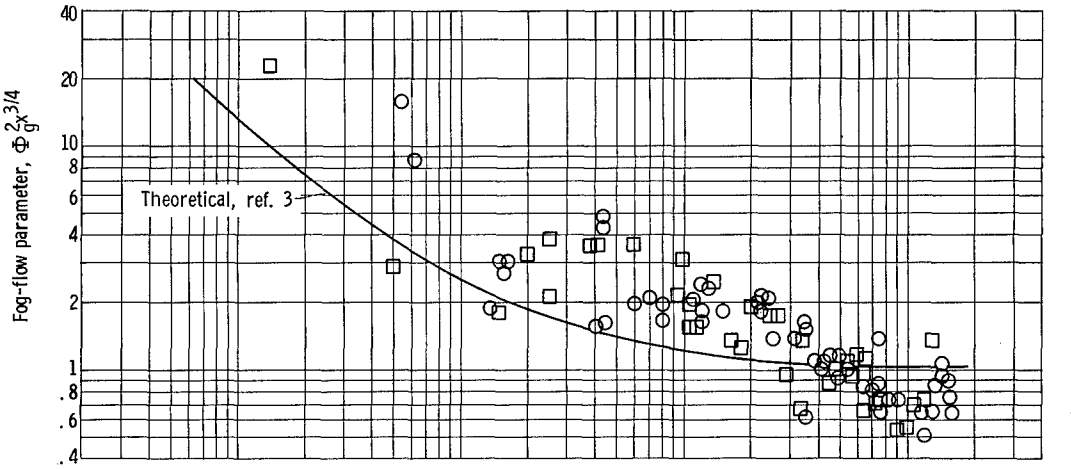

(b) Vapor mass flow rate, 0.035 to 0.038 pound per second; pressure at condensing tube inlet, 15.2 to 17.2 pounds per square inch absolute; temperature at condensing tube inlet, 1010° to 1080° F.

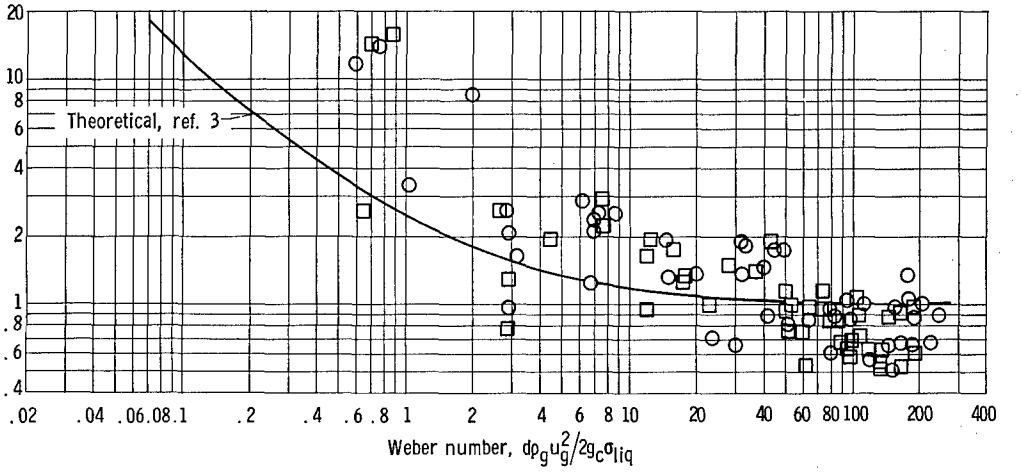

(c) Vapor mass flow rate, 0.044 to 0.048 pound per second; pressure at condensing tube inlet, 14.5 to 18.5 pounds per square inch absolute; temperature at condensing tube inlet, 1000° to 1100° F.

Figure 10. - Comparison of experimental data with fog-flow correlation.

The fog-flow theory roughly predicts the trend of the data over the entire quality range. Experimental values of the fog-flow parameter $\Phi_g^2 x^{3/4}$ varied between -50 and +100 percent of the theoretical value for Weber numbers ranging from 10 to 100 (high velocity region). For Weber numbers ranging from 0.1 to 10 (low velocity region) the experimental values varied between -50 and +165 percent of the theoretical value. The spread in data in the last half of the condensing length can be attributed to the low vapor velocities resulting in small frictional pressure gradients. For example, a 2 percent error in one pressure pickup in this region of the condensing tube can result in a 40 percent change in the frictional pressure gradient.

SUMMARY OF RESULTS

An experimental study of the pressure drop of nonwetting mercury vapor condensing in a uniformly tapered tube in 1-g and zero-gravity environments yielded the following principal results:

1. The gravity effect was negligible for all flow rates investigated.

2. The overall static pressure difference $(P_0 - P_{liq})_S$ varied from a pressure rise of 0.9 pound per square inch to a pressure drop of 0.1 pound per square inch, while the overall total pressure drop varied from 0.0 to 1.4 pounds per square inch for the condensing lengths and flow rates investigated.

3. Lockhart-Martinelli correlation predicts values for the ratio of pressure gradients Φ_g within approximately ±35 percent for the high quality region of the condensing tube. The values of Φ_g ranged up to five times the value predicted by Lockhart-Martinelli for the low quality region of the tube.

4. The fog-flow theory of Koestel, et al. roughly predicts the trend of the data over the entire quality range. Experimental values of the fog-flow parameter $\Phi_g^2 x^{3/4}$ varied between -50 and +100 percent of the theoretical value for Weber numbers ranging from 10 to 100 (high velocity region). For Weber numbers ranging from 0.1 to 10 (low velocity region) the experimental values varied between -50 and +165 percent of the theoretical value.

5. Better agreement with the data was found with the fog-flow theory than with the Lockhart-Martinelli correlation.

Lewis Research Center,
National Aeronautics and Space Administration,
Cleveland, Ohio, September 20, 1965.

APPENDIX A

CALIBRATION

All differential pressure transducers were calibrated simultaneously by pressurizing the mercury system with gaseous nitrogen through the venturi. The low pressure sides of the transducers were all referenced to atmospheric pressure, and a selected range of gage pressure was applied to the system. Desired oscillograph and readout gage spans were adjusted, and recorder runs were made over the calibration range so that transducer calibration curves could be plotted.

The absolute pressure transducers were also calibrated simultaneously by applying pressure to the entire system. In order to zero these transducers, the system was first pumped to a vacuum (1 torr). All other transducers in the system were calibrated individually.

Every high-temperature transducer was calibrated in the system at room temperature before each test run. For the high-temperature transducers in the vapor region, the operating temperature of the diaphragms was estimated to be a maximum of approximately 300° F. The change in output caused by operating at these temperatures was approximately 0.5 percent of the maximum output of the transducers and was considered sufficiently small to neglect when reducing the data.

Temperature indicators on the main control panel needed only periodic inspection for accuracy. The mercury vapor temperature was read on one indicator, and condensing tube wall temperatures were read on a similar indicator by utilizing a selector switch for rapid scanning. Other system temperatures, used mainly for system operation and control, were read out either on controllers or on the temperature oscillograph.

APPENDIX B

LOCAL PRESSURE GRADIENT FOR TAPERED TUBE

When an element of a tapered tube is considered (fig. 11), the sum of forces in the axial direction is:

$$P_1 A_{t,1} - \frac{(P_1 + P_2)}{2}(A_{t,1} - A_{t,2}) - P_2 A_{t,2} = -\frac{1}{g_c} \times (w_{g,1} u_{g,1} - w_{g,2} u_{g,2} + w_{liq,1} u_{liq,1} - w_{liq,2} u_{liq,2}) + F_{TPF} \qquad \text{(B1)}$$

where F_{TPF} is the mean force due to friction within the element. Assuming a velocity ratio of one ($u_{g,1} = u_{liq,1}$, $u_{g,2} = u_{liq,2}$) and simplifying yield

$$(P_1 - P_2) S\left(\frac{A_{t,1} + A_{t,2}}{2}\right) = -\frac{1}{g_c}\left[(w_{g,1} + w_{liq,1}) u_{g,1} - (w_{g,2} + w_{liq,2}) u_{g,2}\right] + F_{TPF} \qquad \text{(B2)}$$

But

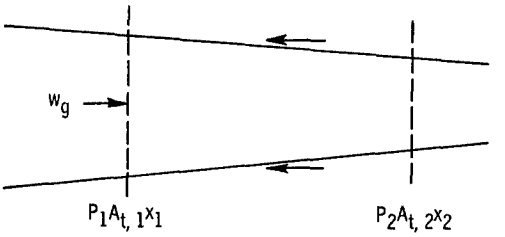

Figure 11. - Element of tapered tube.

and

$$w_T = w_g + w_{liq}$$

$$\bar{A}_t = \frac{A_{t,1} + A_{t,2}}{2}$$

Thus equation (B2) becomes

$$(P_1 - P_2) S \bar{A}_t = -\frac{w_T}{g_c}(u_{g,1} - u_{g,2}) + F_{TPF} \qquad \text{(B3)}$$

If the density changes are assumed small within the increment, the change in velocities becomes

$$u_{g,1} - u_{g,2} = \frac{w_T}{\bar{\rho}} \left(\frac{x_1}{A_{g,1}} - \frac{x_2}{A_{g,2}} \right) \tag{B4}$$

and

$$\bar{\rho} = \frac{\rho_{g,1} + \rho_{g,2}}{2}$$

Substituting equation (B4) into equation (B3) and changing signs yield

$$(P_1 - P_2)_S \bar{A}_t = \frac{w_T^2}{\bar{\rho} g_c} \left(\frac{x_2}{A_{g,2}} - \frac{x_1}{A_{g,1}} \right) + F_{TPF} \tag{B5}$$

where

$$A_g = \frac{A_t}{\frac{1 - x}{x} \frac{\rho_g}{\rho_{liq}} + 1}$$

and F_{TPF} is defined as

$$\frac{\Delta P_{TPF}}{\Delta L} \int_{l_1}^{l_2} A_t dL$$

Then solving for the two-phase frictional pressure gradient $\Delta P_{TPF}/\Delta L$ results in

$$\left(\frac{\Delta P_{TPF}}{\Delta L} \right)_{1,2} = \frac{(P_1 - P_2)_S A_t - \frac{w_T^2}{\bar{\rho} g_c} \left(\frac{x_2}{A_{g,2}} - \frac{x_1}{A_{g,1}} \right)}{\int_{l_1}^{l_2} A_t dL} \tag{B6}$$

where the subscripts 2 and 1 refer to points at one pressure tap and its preceding tap, respectively.

The Fanning equation was used to determine the frictional pressure gradient due to gas alone. It is expressed as

$$\left(\frac{\Delta P_g}{\Delta L}\right) = \frac{4f\rho_g u_g^2}{d2g_c} \tag{B7}$$

where f is the friction factor for turbulent flow in a smooth tube and is expressed as (see ref. 11)

$$f = \frac{0.046}{Re_g^{0.2}} \tag{B8}$$

and

$$u_g = \frac{4w_T x}{\pi\rho_g d^2} \tag{B9}$$

Substituting equations (B8) and (B9) into equation (B7) and integrating to obtain a mean frictional pressure gradient from one pressure tap to the following pressure tap yield the following result:

$$\left(\frac{\Delta P_g}{\Delta L}\right)_{1,2} = \frac{0.092\, w_T^2}{\left(\frac{\pi}{4}\right)^2 g_c\, \Delta L} \int_{l_1}^{l_2} \frac{x^2 dL}{\rho_g Re_g^{0.2} d^5} \tag{B10}$$

For small changes of Reynolds number and density between pressure taps the frictional pressure gradient due to gas alone becomes

$$\left(\frac{\Delta P_g}{\Delta L}\right)_{1,2} = \frac{0.092 w_T^2}{\left(\frac{\pi}{4}\right)^2 g_c \bar{\rho}_g \overline{Re_g^{0.2}}\, \Delta L} \int_{l_1}^{l_2} \frac{x^2}{d^5} dL \tag{B11}$$

where

$$\overline{Re_g^{0.2}} = \frac{\left(Re_g^{0.2}\right)_1 + \left(Re_g^{0.2}\right)_2}{2}$$

The preceding integral was evaluated by numerical integration every inch along the tube length because the diameter and quality are now functions of length.

Equations (B6) and (B11) were used to determine the ratio of the two-phase frictional pressure gradient to the gas phase pressure gradient, where

$$\left(\Phi_g^2\right)_{1,2} = \frac{\left(\frac{\Delta P_{TPF}}{\Delta L}\right)_{1,2}}{\left(\frac{\Delta P_g}{\Delta L}\right)_{1,2}} \qquad \text{(B12)}$$

APPENDIX C

DETERMINATION OF QUALITY AS FUNCTION OF LENGTH FOR TAPERED TUBE

The quality at any point l along the condensing tube is related to the local heat flux q by the following expression:

$$x = x_0 - \frac{\int_0^l q\pi D\, dL}{w_T\left[h_{fg} + c_p(T_{sup} - T_{sat})\right]} \tag{C1}$$

The heat flux at any point l along the tube is expressed as

$$q = h_{N_2}\left(T_w - T_{N_2}\right) \tag{C2}$$

If the wall temperature and the coolant temperature are both assumed nearly constant along the condensing tube length (small pressure changes), the average heat flux can be expressed as

$$\bar{q} = \left(T_w - T_{N_2}\right)\overline{h_{N_2}} \tag{C3}$$

The cooling gas side heat-transfer coefficient is determined from Hilbert's equation for gas flowing perpendicular to cylinders (ref. 11)

$$Nu = BRe^n = B\left(\frac{\rho_{N_2} u_{N_2} D}{\mu_{N_2}}\right)^n \tag{C4}$$

where B and n are dimensionless constants depending on the value of Re. Assuming that the mass velocity $\rho_{N_2} u_{N_2}$ and μ_{N_2} of the nitrogen coolant are constant along the condensing tube yields

$$Nu = B'D^n = \frac{h_{N_2} D}{k_{N_2}} \tag{C5}$$

where

$$B' = B\left(\frac{\rho_{N_2} u_{N_2}}{\mu_{N_2}}\right)^n$$

Assuming k_{N_2} constant and solving for h_{N_2} give

$$h_{N_2} = \frac{B''D^n}{D} = B''D^{n-1} \tag{C6}$$

where

$$B'' = k_{N_2} B'$$

Similarly, the average cooling side heat-transfer coefficient becomes

$$\overline{h_{N_2}} = B'' \overline{D^{n-1}} = B'' \frac{1}{l_c} \int_0^{l_c} D^{n-1} dL \tag{C7}$$

From equation (C3) and (C7) the integrated heat flux can be expressed as

$$\bar{q} = \left(T_w - T_{N_2}\right) B'' \frac{1}{l_c} \int_0^{l_c} D^{n-1} dL \tag{C8}$$

Dividing equation (C6) by (C7) yields

$$\frac{h_{N_2}}{\overline{h_{N_2}}} = \frac{l_c D^{n-1}}{\int_0^{l_c} D^{n-1} dL} \tag{C9}$$

and solving for h_{N_2} gives

$$h_{N_2} = \overline{h_{N_2}} \frac{l_c D^{n-1}}{\int_0^{l_c} D^{n-1} dL} \tag{C10}$$

Placing equation (C3) into equation (C10) results in

$$h_{N_2} = \frac{\bar{q}}{\left(T_w - T_{N_2}\right)} \frac{l_c D^{n-1}}{\int_0^{l_c} D^{n-1} dL} \tag{C11}$$

The heat flux at any point along the tube is determined by equation (C2) and (C11). Then

$$q = \bar{q} \frac{l_c D^{n-1}}{\int_0^{l_c} D^{n-1} dL} \tag{C12}$$

The average heat flux can be expressed as

$$\bar{q} = \frac{w_T x_0 \left[h_{fg} + c_p (T_{sup} - T_{sat})\right]}{\pi \bar{D} l_c} \tag{C13}$$

where

$$\bar{D} = \frac{(D_0 + D_c)}{2}$$

Equating the average heat flux in equation (C13) to the integrated heat flux defined in equation (C8) and then substituting equation (C13) into (C12) yield the following expression for local heat flux:

$$q = \frac{w_T x_0 \left[h_{fg} + c_p (T_{sup} - T_{sat}) \right] D^{n-1}}{\pi \overline{D} \int_0^{l_c} D^{n-1} \, dL} \tag{C14}$$

The quality can be expressed as a function of the diameter by placing (C14) into equation (C1) and simplifying:

$$x = x_0 - x_0 \frac{\int_0^{l} D^{n-1} D \, dL}{\overline{D} \int_0^{l_c} D^{n-1} \, dL} \tag{C15}$$

or

$$x = x_0 \left(1 - \frac{\int_0^{l} D^{n} \, dL}{\overline{D} \int_0^{l_c} D^{n-1} \, dL} \right) \tag{C16}$$

where the diameter varies linearly along the tube

$$D = C_1 + C_2 L \tag{C17}$$

Then the quality is expressed as a function of length:

$$x = x_0 \left[1 - \frac{\int_0^{l} (C_1 + C_2 L)^n \, dL}{\overline{D} \int_0^{l_c} (C_1 + C_2 L)^{n-1} \, dL} \right] \tag{C18}$$

Since from the table of integrals

$$\int (a + bx)^c \, dx = \frac{(a + bx)^{c+1}}{(c + 1)b}$$

then

$$x = x_0\left\{1 - \frac{\left[\frac{(C_1 + C_2L)^{n+1}}{(n+1)C_2}\right]_0^{l}}{\overline{D}\left[\frac{(C_1 + C_2L)^{n}}{nC_2}\right]_0^{l_c}}\right\} \tag{C19}$$

When the limits of integration are inserted, equation (C19) is expressed as

$$x = x_0\left\{1 - \frac{\left[\frac{(C_1 + C_2 l)^{n+1} - C_1^{n+1}}{(n+1)C_2}\right]}{\overline{D}\left[\frac{(C_1 + C_2 l_c)^{n} - C_1^{n}}{nC_2}\right]}\right\} \tag{C20}$$

where

$$\left.\begin{aligned} C_1 &= D_0 \\ C_2 &= -\frac{(D_0 - D_e)}{l_e} \\ \overline{D} &= \frac{(D_0 + D_c)}{2} \end{aligned}\right\} \tag{C21}$$

Substituting equation (C21) into (C20) yields the following

$$x = x_0\left(1 - \frac{2n\left\{\left[D_0 - (D_0 - D_e)\frac{l}{l_e}\right]^{n+1} - D_0^{n+1}\right\}}{(n+1)\left\{\left[D_0 - (D_0 - D_e)\frac{l_c}{l_e}\right]^{n} - D_0^{n}\right\}(D_0 + D_c)}\right) \tag{C22}$$

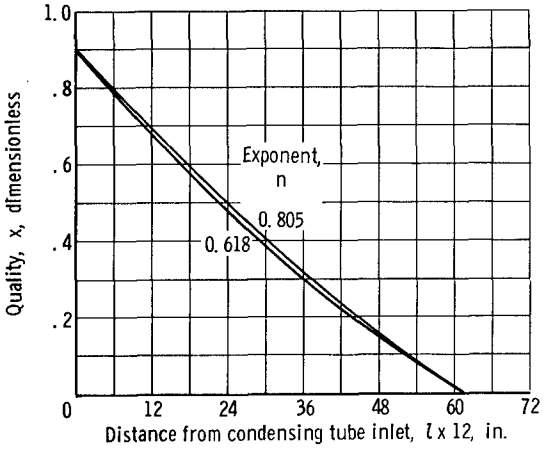

Figure 12. - Quality distribution along condensing tube for values of exponent n.

The exponent n can be determined from the average Nusselt number for the condensing tube, where

$$\overline{Nu} = \frac{\overline{h_{N_2}}\,\overline{D}}{k_{N_2}} \tag{C23}$$

From equations (C3) and (C13) the average cooling heat-transfer coefficient for a given flow rate and condensing length is expressed as

$$\overline{h_{N_2}} = \frac{w_T x_0 \left[h_{fg} + c_p(T_{sup} - T_{sat})\right]}{\pi \overline{D} l_c \left(T_w - T_{N_2}\right)} \tag{C24}$$

Then

$$\overline{Nu} = \frac{w_T x_0 \left[h_{fg} + c_p(T_{sup} - T_{sat})\right]}{\pi l_c k_{N_2} \left(T_w - T_{N_2}\right)} \tag{C25}$$

For the flow rates and condensing lengths considered the average Nusselt number varied from approximately 100 to 230.

From reference 11 the exponent n in equation (C22) is equal to the following values: Nu = 29.5 to 121 where n = 0.618; Nu = 121 to 528 where n = 0.805. The difference in the variation of quality against length for values of the exponent n equal to 0.618 and 0.805 is negligible (fig. 12).

If a value of n = 0.805 is assumed, the distribution of quality can be determined from equation (C22):

$$x = x_0 \left(1 - \frac{1.61\left\{\left[D_0 - (D_0 - D_e)\frac{l}{l_e}\right]^{1.805} - D_0^{1.805}\right\}}{1.805\left\{\left[D_0 - (D_0 - D_e)\frac{l_c}{l_e}\right]^{0.805} - D_0^{0.805}\right\}(D_0 + D_c)} \right) \tag{C26}$$

APPENDIX D

DETERMINATION OF CONDENSER INLET QUALITY

Determination of inlet quality requires measurement of inlet vapor flow rate and total flow rate. The total flow rate was determined from the pressure drop ΔP_2 across a calibrated orifice at the preheater inlet. Vapor flow rate at the condenser inlet was measured by means of a venturi meter. Such measurements, however, involve determining the contribution of liquid carryover to the measurement. An investigation of the amount of liquid content that significantly affects pressure readings was made by Murdock (ref. 9). He derived expressions (based on experimental data) for total flow rate and two-phase pressure drop through an orifice meter. The total flow through an orifice meter is given by the expression

$$w_T = \frac{K_g Y_g A_{th} \sqrt{2g_c \, \Delta P_{TP} \rho_g}}{x + \dfrac{1.26(1 - x) K_g Y_g}{K_{liq}} \sqrt{\dfrac{\rho_g}{\rho_{liq}}}} \tag{D1}$$

where

A_{th} cross-sectional area of throat, sq ft

K flow coefficient, dimensionless

Y net expansion factor, dimensionless

Because of the low values of vapor-to-liquid-density ratios for mercury (3×10^{-4}), the second term of the denominator can be neglected for the high inlet qualities considered (85 percent and above). Equation (D1) when solved for inlet quality becomes

$$x = \frac{K_g Y_g A_{th} \sqrt{2g_c \, \Delta P_{TP} \rho_g}}{w_T} \tag{D2}$$

In a like manner the relation between $\sqrt{\Delta P_g}$ and $\sqrt{\Delta P_{TP}}$ becomes (see ref. 9)

$$\sqrt{\Delta P_g} = \frac{\sqrt{\Delta P_{TP}}}{1 + \dfrac{1.26 K_g Y_g (1 - x)}{x K_{liq}} \sqrt{\dfrac{\rho_g}{\rho_{liq}}}} \tag{D3}$$

For qualities 85 percent or above the two-phase pressure drop is equal to the one-phase pressure drop because of the low value of the vapor-to-liquid-density ratio for mercury. Then equation (D3) reduces to

$$\Delta P_g = \Delta P_{TP} \tag{D4}$$

Thus, the influence of liquid carryover on the measured pressure drop was small and can be neglected. The inlet quality can then be expressed as

$$x = \frac{K_g Y_g A_{th} \sqrt{2 g_c \Delta P_g \rho_g}}{w_T} \tag{D5}$$

where the numerator of equation (D5) is the standard equation for calculating the vapor flow rate through a venturi (ref. 12). If steady flow through the boiler is assumed, the inlet quality can be expressed as the ratio of the vapor flow rate out of the boiler (measured by the venturi) to the total liquid flow rate into the boiler. Previous boiler performance tests indicated no liquid holdup in the boiler. Then

$$x_0 = \frac{w_g}{w_T} \tag{D6}$$

It is assumed that the liquid droplets in the venturi do not vaporize because of the small pressure drop through the venturi (2 to 3 psi), short residence time, and high surface tension of the liquid droplets.

REFERENCES

1. Albers, James A.; and Macosko, Robert P.: Experimental Pressure-Drop Investigation of Nonwetting, Condensing Flow of Mercury Vapor in a Constant-Diameter Tube in 1-G and Zero-Gravity Environments. NASA TN D-2838, 1965.
2. Lockhart, R.W.; and Martinelli, R.C.: Proposed Correlation of Data for Isothermal Two-Phase, Two-Component Flow in Pipes. Chem. Eng. Prog., vol. 45, no. 1, 1949, pp. 39-48.
3. Koestel, Alfred; Gutstein, Martin U.; and Wainwright, Robert T.: Study of Wetting and Nonwetting Mercury Condensing Pressure Drops. NASA TN D-2514, 1964.
4. Hays, L.: Investigation of Condensers Applicable to Space Power Systems. Pt. 1. Direct Condensers. NASA CR-51397, 1962.
5. Kiraly, R.J.; and Koestel, A.: The SNAP-II Power Conversion System Topical Report No. 8. Mercury Condensing Research Studies. Rept. No. ER-4442, Thompson Ramo Wooldridge, Inc., May 31, 1961.
6. Jaenke, C.T.; Koestel, A.; and Reitz, J.G.: The SNAP-II Power Conversion System Topical Report No. 13. Orbital Force Field Boiling and Condensing Experiments (Offbace). Rept. No. ER-4670, Thompson Ramo Wooldridge, Inc., Oct. 1962.
7. Jakob, Max: Heat Transfer in Evaporation and Condensation, II. Mech. Eng., vol. 58, no. 11, Nov. 1936, pp. 729-739.
8. Kutateladze, S.S. (S.J. Rimshaw, trans.): Heat Transfer in Condensation and Boiling. Rept. No. TR-3770, AEC, 1952, pp. 53-60.
9. Murdock, J.W.: Two-Phase Flow Measurement with Orifices. J. Basic Eng. (ASME Trans.), ser. D, vol. 84, no. 2, Dec. 1962, pp. 419-433.
10. Weatherford, W.D., Jr.; Tyler, J.C.; and Ku, P.M.: Properties of Inorganic Energy-Conversion and Heat-Transfer Fluids for Space Applications. Rept. No. TR 61-96, WADD, Nov. 1961.
11. McAdams, W.H.: Heat Transmission. Third ed., McGraw-Hill Book Co., Inc., 1954.
12. Anon.: Power Test Codes - Instruments and Apparatus. ASME, 1959, pt. S, ch. 4.

TABLE I. - TRANSDUCER CALIBRATION RANGE

Pressure transducer	Description	Calibration range, psi	Temperature region
PT_0	Pressure at venturi exit	[a]0 to 4	High temperature
PT_1	Explusion pressure	[b]0 to 200	Low temperature
PT_2	Pressure drop across orifice	[a]0 to 80	Low temperature
PT_3	Pressure between preheated and high flux boiler	[b]0 to 150	Low temperature
PT_4	Venturi inlet pressure	[b]0 to 30	High temperature
PT_5	Venturi pressure drop	[a]0 to 4	High temperature
PT_6	Mercury receiver pressure	[b]0 to 30	Low temperature
PT_7	Reference manifold pressure	[b]0 to 30	Low temperature
PT_{12}	Pressure 12 in. from condensing tube inlet	[a]0 to 4	High temperature
PT_{36}	Pressure 36 in. from condensing tube inlet	[a]0 to 4	↓
PT_{48}	Pressure 48 in. from condensing tube inlet	[a]0 to 4	
PT_{60}	Pressure 60 in. from condensing tube inlet	[a]0 to 4	
PT_{72}	Pressure 72 in. from condensing tube inlet	[a]0 to 4	

[a]Differential.
[b]Absolute.

TABLE II. - EXPERIMENTAL DATA

Gravity level, g's	Point identification [a]	Condensing length, $l_c \times 12$, in.	Liquid mass flow rate, w_{liq}, lb/sec	Vapor mass flow rate, w_g, lb/sec	Inlet quality, x_0	Static pressure, $P_S/144$, psia						
						[b]P_0	P_{12}	P_{36}	P_{48}	P_{60}	P_{72}	Temperature at condensing tube inlet, T_0, °F
1	1	51	0.0418	0.0386	0.92	19.29	18.54	18.50	18.80	19.70	19.50	1020
0	1A	51	.0488	.0442	.91	18.96	18.10	18.33	18.85	19.10	18.80	1040
1	2	51	.0415	.0372	.90	16.50	15.80	15.95	16.70	17.25	17.15	1040
0	2A	51	.0469	.0418	.89	16.60	16.05	16.10	16.90	16.65	16.35	1050
0	3A	41	.0426	.0357	.84	15.74	15.53	15.73	16.43	16.48	16.37	1070
1	4	43	.0396	.0361	.91	15.69	15.52	15.62	16.18	16.73	16.53	1060
0	4A	41	.0400	.0352	.88	15.67	15.45	15.55	16.25	16.45	16.25	1050
1	5	47	.0417	.0367	.88	15.73	15.48	15.33	15.78	16.69	16.50	1050
1	6	57	.0417	.0376	.90	15.30	14.94	14.54	14.67	15.28	16.16	1050
1	7	63	.0386	.0365	.94	16.10	15.58	15.21	15.11	15.68	16.65	1020
0	7A	63	.0423	.0360	.85	16.24	15.73	15.43	15.43	16.07	16.48	1040
1	8	59	.0404	.0371	.92	16.77	16.31	15.90	15.67	16.30	17.25	1060
0	8A	61	.0405	.0365	.90	16.77	16.20	15.78	15.58	16.20	17.00	1060
1	9	53	.0386	.0350	.91	15.19	14.93	14.63	14.73	16.18	15.98	1070
0	9A	53	.0414	.0370	.89	15.61	15.16	14.94	15.04	16.18	15.98	1080
1	10	49	.0399	.0360	.90	14.97	14.79	14.68	14.91	16.08	15.88	1070
0	10A	45	.0408	.0367	.90	15.36	15.00	14.95	15.25	16.20	16.00	1080
1	11	42	.0396	.0360	.91	14.53	14.38	14.76	15.43	15.88	15.78	1080
0	11A	41	.0407	.0362	.89	15.08	14.75	15.06	15.72	15.95	15.75	1080
1	12	37	.0398	.0362	.91	16.15	16.05	16.40	16.82	17.00	16.80	1080
0	12A	41	.0413	.0367	.89	15.53	15.15	15.43	16.13	16.36	16.16	1080
1	13	43	.0385	.0351	.91	15.48	15.10	15.20	16.00	16.60	16.40	1080
0	13A	45	.0402	.0366	.91	15.40	15.00	14.90	15.10	16.05	15.85	1080
1	14	65	.0291	.0272	.94	18.23	18.10	17.75	17.70	17.93	18.42	1010
0	14A	65	.0280	.0280	1.00	18.85	18.68	18.23	18.26	18.80	18.85	1020
1	15	69	.0299	.0260	.87	17.43	17.44	17.08	16.85	17.20	17.70	1020
0	15A	69	.0288	.0288	1.00	18.95	18.62	18.17	18.08	18.37	18.84	1030
1	16	55	.0300	.0263	.88	17.77	17.64	17.40	17.51	17.88	18.04	1020
0	16A	55	.0290	.0265	.91	19.02	18.85	18.47	18.64	19.00	19.05	1030
1	17	49	.0300	.0267	.89	18.79	18.71	18.55	18.90	18.96	18.93	1020
0	17A	49	.0290	.0260	.90	19.70	19.57	19.37	19.72	19.77	19.87	1040
1	18	43	.0300	.0261	.87	18.30	18.25	18.18	18.46	18.50	18.69	1040
0	18A	43	.0294	.0265	.90	19.97	19.81	19.58	19.96	19.93	19.97	1040
1	19	45	.0300	.0268	.89	19.44	19.31	19.22	19.53	19.68	19.85	1020
0	19A	45	.0296	.0266	.90	20.19	19.98	19.90	20.21	20.15	20.18	1040

[a]Number designates trajectory; A, middle portion of trajectory; B, late portion of trajectory.
[b]Corrected.

TABLE II. - Continued. EXPERIMENTAL DATA

Gravity level, g's	Point identification [a]	Condensing length, $l_c \times 12$, in.	Liquid mass flow rate, w_{liq}, lb/sec	Vapor mass flow rate, w_g, lb/sec	Inlet quality, x_0	Static pressure, $P_S/144$, psia						
						[b]P_0	P_{12}	P_{36}	P_{48}	P_{60}	P_{72}	Temperature at condensing tube inlet, T_0, ^oF
1	20	39	0.0300	0.0270	0.90	18.78	18.70	18.65	18.83	18.78	18.85	1020
0	20A	37	.0291	.0252	.87	20.19	20.07	19.92	20.17	20.10	20.18	1040
1	21	41	.0300	.0273	.91	20.17	19.59	19.49	19.65	19.60	19.71	1020
0	21A	43	.0293	.0266	.91	20.53	20.48	20.21	20.53	20.51	20.54	1040
1	22	63	.0514	.0464	.90	21.68	21.20	20.49	20.35	21.02	22.35	1040
0	22A	64	.0504	.0452	.90	22.20	21.78	20.99	20.89	21.68	22.68	1060
1	23	67	.0501	.0454	.91	22.80	22.18	21.42	21.19	21.78	23.16	1090
0	23A	71	.0507	.0456	.90	20.81	20.16	19.26	18.95	19.54	21.08	1100
1	24	55	.0500	.0455	.91	19.43	19.05	18.65	18.83	20.41	20.29	1030
0	24A	55	.0513	.0462	.90	19.51	18.91	18.51	18.79	20.03	19.94	1040
1	25	51	.0506	.0463	.92	20.88	20.58	20.42	21.47	20.72	20.52	1020
1	26	65	.0408	.0375	.92	16.04	15.67	15.02	14.70	15.30	16.59	955
0	26A	71	.0387	.0377	.97	16.51	16.08	15.54	15.15	15.68	16.82	1000
0	26B	71	.0389	.0404	1.00	16.67	16.05	15.21	14.90	15.42	16.72	1000
1	27	71	.0394	.0376	.95	16.22	15.90	15.00	14.62	15.00	16.70	1030
1	28	61	.0410	.0389	.94	15.20	14.75	14.10	13.80	14.45	15.95	1040
0	28A	61	.0394	.0375	.95	15.75	15.40	14.70	14.60	15.60	16.20	1040
0	28B	61	.0396	.0372	.94	15.99	15.53	14.81	14.63	15.40	16.24	1040
1	29	57	.0414	.0376	.91	15.86	15.70	15.02	15.02	15.03	16.05	1010
0	29A	57	.0402	.0380	.94	15.50	15.20	14.45	14.38	15.80	15.13	1020
0	29B	57	.0402	.0379	.97	15.60	15.18	14.55	14.48	15.90	15.83	1040
1	30	51	.0402	.0372	.93	15.53	15.40	14.97	15.16	16.26	16.26	1030
0	30A	51	.0410	.0373	.91	15.81	15.44	15.09	15.31	16.42	16.40	1040
0	30B	51	.0410	.0377	.92	15.58	15.30	14.90	15.13	16.13	16.08	1040
1	31	63	.0405	.0373	.92	15.73	15.53	14.75	14.44	15.08	16.46	1040
0	31	63	.0405	.0364	.90	16.06	15.55	14.80	14.45	14.85	16.25	1040
1	32	63	.0305	.0274	.90	12.81	12.58	12.23	12.08	12.58	13.06	1000
0	32	61	.0300	.0282	.94	13.54	13.10	12.80	12.65	13.15	13.57	1020
1	33	55	.0305	.0263	.87	13.53	13.30	13.10	13.10	13.70	13.70	1020
0	33	55	.0308	.0278	.90	13.78	13.41	13.08	13.20	14.02	13.82	1030
1	34	51	.0305	.0265	.87	12.44	12.22	12.15	12.18	13.20	13.05	1030
0	34	51	.0301	.0270	.90	13.88	13.63	13.53	13.53	14.28	14.08	1040
1	35	43	.0312	.0276	.88	12.85	12.75	12.73	12.93	13.47	13.35	1010
0	35	44	.0311	.0270	.87	13.84	13.50	13.58	13.92	14.12	14.10	1020
1	36	41	.0316	.0282	.89	12.64	12.51	12.67	12.84	13.28	13.13	980

[a]Number designates trajectory; A, middle portion of trajectory; B, late portion of trajectory.
[b]Corrected.

TABLE II. - Concluded. EXPERIMENTAL DATA

Gravity level, g's	Point identification (a)	Condensing length, $l_c \times 12$, in.	Liquid mass flow rate, w_{liq}, lb/sec	Vapor mass flow rate, w_g, lb/sec	Inlet quality, x_0	Static pressure, $P_S/144$, psia						
						[b]P_0	P_{12}	P_{36}	P_{48}	P_{60}	P_{72}	Temperature at condensing tube inlet, T_0, °F
0	36	41	0.0320	0.0275	0.86	13.24	13.00	13.15	13.37	13.60	13.50	980
1	37	47	.0321	.0273	.85	12.85	12.73	12.70	12.76	13.98	13.38	930
0	37	53	.0321	.0271	.84	13.82	13.48	13.38	13.58	14.03	13.88	930
1	38	70	.0298	.0263	.88	15.15	14.85	14.53	14.24	14.63	15.20	1010
0	38	70	.0284	.0274	.96	15.85	15.53	15.10	14.80	15.10	15.75	1020
1	39	64	.0297	.0266	.90	14.71	14.48	14.20	14.00	14.15	14.99	1030
0	39	65	.0298	.0270	.90	15.30	15.05	14.74	14.60	14.94	15.22	1030
1	40	55	.0285	.0260	.91	15.06	14.94	14.65	14.65	15.49	15.35	1040
0	40	57	.0295	.0268	.91	15.68	15.33	15.00	14.89	15.80	15.63	1040
1	41	52	.0301	.0270	.90	15.15	14.98	14.78	14.76	15.70	15.34	1040
0	41	52	.0301	.0272	.90	15.32	14.99	14.75	14.65	15.55	15.35	1040
1	42	55	.0402	.0365	.91	16.64	16.53	16.11	15.81	17.41	17.36	1080
0	42	57	.0400	.0362	.91	-----	16.15	15.75	14.47	15.90	15.70	1080
1	43	51	.0394	.0359	.91	15.18	14.83	14.52	14.62	15.82	15.69	1080
0	43	51	.0395	.0354	.90	15.56	15.25	14.85	14.90	16.15	15.95	1080
1	44	51	.0406	.0365	.90	15.21	15.10	14.70	14.77	16.13	15.88	1080
0	44	51	.0302	.0280	.93	-----	14.63	14.49	14.57	15.63	15.43	1080
1	45	70	.0491	.0469	.95	14.76	13.79	12.57	12.37	13.35	15.07	1000
0	45	70	.0481	.0435	.90	14.69	13.88	12.88	12.55	13.18	14.98	1040
1	46	59	.0504	.0445	.88	16.94	16.33	15.81	15.83	17.43	17.33	1060
0	46	59	.0481	.0447	.93	17.44	16.58	15.98	16.08	17.57	17.37	1090
1	47	51	.0513	.0457	.89	17.11	16.60	16.60	17.80	17.98	17.84	1040
0	47	51	.0514	.0458	.89	17.02	16.20	16.30	17.50	17.62	17.38	1030
1	48	45	.0501	.0446	.89	17.40	17.09	17.27	18.20	18.45	18.29	960
0	48	47	.0481	.0438	.91	17.19	16.65	16.75	17.83	17.95	17.66	1000
1	49	63	.0505	.0452	.89	17.96	17.46	16.58	16.32	17.08	18.58	1060
0	49	84	.0513	.0460	.90	19.20	18.40	17.03	16.03	15.73	14.53	1060
1	50	54	.0512	.0460	.90	17.25	16.65	15.95	15.95	17.85	17.85	1100
0	50	54	.0520	.0468	.90	16.42	15.76	15.41	15.47	17.10	16.90	1070
1	51	56	.0512	.0453	.88	17.18	16.68	16.02	16.08	17.88	17.78	1070
0	51	54	.0535	.0465	.87	17.67	17.20	16.52	16.51	18.43	18.33	1070
0	52	70	.0524	.0460	.88	18.10	17.01	15.53	15.35	15.73	17.38	1060
1	52	63	.0505	.0450	.89	16.17	15.52	14.87	-----	16.90	16.70	1030
0	53	65	.0477	.0438	.92	16.36	15.51	14.87	14.83	16.48	16.39	1060
1	54	49	.0527	.0452	.86	15.68	14.96	15.00	16.29	16.50	16.30	960

[a]Number designates trajectory; A, middle portion of trajectory; B, late portion of trajectory.
[b]Corrected.

"The aeronautical and space activities of the United States shall be conducted so as to contribute . . . to the expansion of human knowledge of phenomena in the atmosphere and space. The Administration shall provide for the widest practicable and appropriate dissemination of information concerning its activities and the results thereof."

—NATIONAL AERONAUTICS AND SPACE ACT OF 1958

NASA SCIENTIFIC AND TECHNICAL PUBLICATIONS

TECHNICAL REPORTS: Scientific and technical information considered important, complete, and a lasting contribution to existing knowledge.

TECHNICAL NOTES: Information less broad in scope but nevertheless of importance as a contribution to existing knowledge.

TECHNICAL MEMORANDUMS: Information receiving limited distribution because of preliminary data, security classification, or other reasons.

CONTRACTOR REPORTS: Technical information generated in connection with a NASA contract or grant and released under NASA auspices.

TECHNICAL TRANSLATIONS: Information published in a foreign language considered to merit NASA distribution in English.

TECHNICAL REPRINTS: Information derived from NASA activities and initially published in the form of journal articles.

SPECIAL PUBLICATIONS: Information derived from or of value to NASA activities but not necessarily reporting the results of individual NASA-programmed scientific efforts. Publications include conference proceedings, monographs, data compilations, handbooks, sourcebooks, and special bibliographies.

Details on the availability of these publications may be obtained from:

SCIENTIFIC AND TECHNICAL INFORMATION DIVISION

NATIONAL AERONAUTICS AND SPACE ADMINISTRATION

Washington, D.C. 20546